ELSEVIER

Journal of Atmospheric and Solar-Terrestrial Physics 66 (2004) 1491–1497

Journal of ATMOSPHERIC AND SOLAR-TERRESTRIAL PHYSICS

www.elsevier.com/locate/jastp

Sun-to-magnetosphere modeling: CISM forecast model development using linked empirical methods

D.N. Baker[a,*], R.S. Weigel[a], E.J. Rigler[a], R.L. McPherron[b], D. Vassiliadis[c], C.N. Arge[d], G.L. Siscoe[e], H.E. Spence[e]

[a]*Laboratory for Atmospheric and Space Physics, University of Colorado at Boulder, CO, USA*
[b]*IGPP/University of California at Los Angeles, USA*
[c]*USRA/NASA Goddard SFC, USA*
[d]*Air Force Research Laboratory, Hanscom AFB, MA, USA*
[e]*Boston University, Boston, MA, USA*

Received 28 January 2004; received in revised form 1 April 2004; accepted 1 April 2004
Available online 3 September 2004

Abstract

The Wang–Sheeley–Arge (WSA) method is used to predict the solar wind speed (and certain other parameters) near the Earth's orbit based upon solar surface measurements. This approach gives a predicted solar wind time series with a lead time of three to four days. Such forecasted solar wind conditions can then be convolved with linear and nonlinear filters in order to provide a predicted set of geomagnetic indices or various particle flux estimates. In order to illustrate the method in a concrete way, we present here a demonstration of an end-to-end empirical forecast of relativistic electrons in the outer Van Allen radiation belt. Past work has shown that radiation belt electron fluxes are highly dependent on the speed of the solar wind striking the magnetosphere. We develop filters that predict electron fluxes using the WSA estimates of solar wind speed at L1, which allows for 3–4 days lead times. We compare the prediction efficiency (PE) provided by these filters with filters developed to use 3–4 day old values of the solar wind velocity measured at L1 and 3–4 day old values of the measured electron fluxes themselves. It is found that the WSA method provides PEs of the electron flux that are slightly lower than that provided by using old L1 or the autocorrelated electron flux data.

Keywords: Space weather; Radiation belts; Forecast models; Energetic electrons

1. Introduction

A key goal of the Center for Integrated Space Weather Modeling (CISM) is to provide linked end-to-end models of the connected Sun–Earth system. It is envisioned that the ultimate product of the CISM effort will be a single, physics-based (i.e., "forward") model which will describe with requisite accuracy the origin and evolution of solar wind elements, the propagation of these solar wind elements from the Sun out to the Earth's environs, and the subsequent interaction of the solar wind with the coupled magnetosphere–ionosphere–atmosphere system. It is presently expected that the backbone of this coupled model will be based on magnetohydrodynamic (MHD) numerical codes (e.g.,

*Corresponding author. Tel.: +1-303-492-4509; fax: +1-303-735-4843.
E-mail address: daniel.baker@lasp.colorado.edu (D.N. Baker).

1364-6826/$ - see front matter © 2004 Elsevier Ltd. All rights reserved.
doi:10.1016/j.jastp.2004.04.011

Luhmann and Solomon, this issue; Wiltberger et al., this issue). Considerable work must yet be done to assure that such forward models can provide a complete, accurate and robust description of the Sun–Earth system under all conditions.

Given the challenges of producing an efficient, effective end-to-end physics-based model at the present time, the CISM team has chosen to utilize empirical, semi-empirical, and inverse models to provide a present-day, state-of-the-art forecast model (FM) of the Sun–Earth system. As shown by the lower part of the flow diagram in Fig. 1, it is possible to use previously-developed empirical methods to observe the Sun, specify the solar boundary conditions, follow the subsequent solar wind propagation to 1 astronomical unit (AU), and thereby forecast key solar wind parameters such as mass density (ρ), speed (V), and magnetic field strength (B). With such parameters forecasted in the immediate vicinity of Earth's dayside magnetopause, it is further possible to predict a variety of useful quantities such as geomagnetic indices (e.g., Ap, Kp, or Dst), magnetic field fluctuations at mid- and high-latitudes, global magnetospheric field configurations (using the Tsyganesko models), and the relativistic electron fluxes in the Earth's radiation belts.

As illustrated in Fig. 1 (top part of figure), it has been much more common in the past to use measurements from a solar wind monitor at the upstream Lagrangian point (L1) to drive empirical forecast models (see, for example, Tsurutani and Baker, 1979). However, using L1 data typically allows for only a 30–60 min lead time for forecasting. The CISM team has chosen to explore the possibility of pushing the methods back as far as possible in time in order to give three- to four-day lead times.

A further point to note with respect to Fig. 1 is quite important: The empirical end-to-end models being developed and tested today by CISM have enduring utility. The current performance of such models will be the baseline against which the physics-based (PB) models are compared now and in the future. It is envisaged that the numerical models, at least initially, will not perform as well as the highly tuned, quite specialized empirical models (EMs), or the "inverse" models that were developed in locations that have a long record of historical data available (Weigel et al., 2003; Vassiliadis et al., 2002). However, as time goes on, it is expected that the PB models will improve and—it is hoped—will in many cases outperform the existing models. A key aspect of the National Space Weather Program (NSWP, 1995) is to provide metrics to judge model performance and improvement. The EM baseline will provide a comparator against which PB models and the composite FM can be judged now and over the course of the CISM program (see Spence et al., 2004).

This paper will describe our initial Sun-to-Earth model development and performance characteristics. In order to illustrate the ideas with specificity, we will present our results for the forecasting of radiation belt electron fluxes. Given the key space weather significance of such electrons (e.g., Baker, 1998; Li et al., 2003), it seems appropriate to use this aspect of the space environment to illustrate our approach. We will demonstrate here that present-day end-to-end prediction efficiencies are not yet very high. Thus, much work needs to be done even for linked empirical models to achieve the kind of model accuracy desired by the NSWP (1995).

2. Data and models for the Sun-to-Earth chain

Taking Fig. 1 as a guide, an end-to-end model requires information about the solar surface and corona which provides the 'initial' conditions for the model. The Wang–Sheeley method (e.g., Wang et al., 2002 and references therein) uses source surface maps of the solar magnetic field from the Mount Wilson Observatory magnetograms. This method then allows an inference of the solar wind speed and some aspects of the interplanetary magnetic field (IMF) which may be kinematically projected outward to 1 AU. The Wang–Sheeley approach has been modified and improved by Arge and Pizzo (2000). This so-called Wang–Sheeley–Arge (WSA) method is also being used to help drive and constrain CISM interplanetary MHD codes (Arge and Odstrcil,

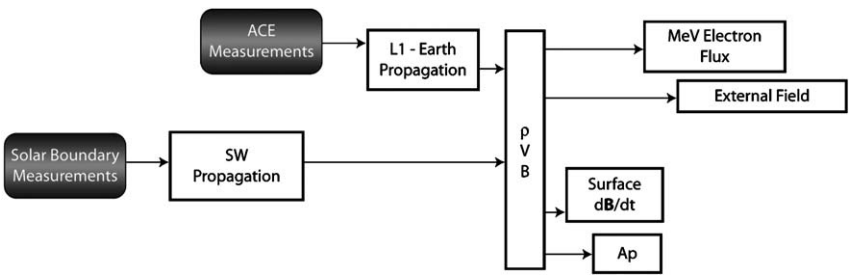

Fig. 1. Linked empirical models being developed within the CISM framework in order to provide forecasts of key parameters and indices as shown to the right.

this issue) with realistic initial conditions and a geomagnetic activity model.

The WSA model provides the results needed for the "Solar Boundary Measurement" and the "SW Propagation" boxes in Fig. 1. The output of the model is principally the predicted value of solar wind speed, V_{SW}, at the Earth. The forecasted value of V_{SW} has a lead time of 3–4 days, which corresponds to typical sun–Earth propagation times. The predicted value of V_{SW} can then be used as a "driver" for downstream models (as shown by the boxes on the right-hand side of Fig. 1). In this paper we will illustrate the method by specifying and forecasting energetic electrons in the outer radiation belt. As shown in Fig. 2, the observations of magnetic field on the Sun ($B_{sun}(\tau < t-4)$) for time τ prior to the current time t, with the kinematic propagation operator (f) that represents the WSA method, gives a time series

$$V_{SW}(t) = f(B_{sun}(\tau < t-4), R) \quad (1)$$

for any radial location R. Note that the actual arrival time varies, so $V_{SW}(t)$ is typically computed based on solar observations 3–5 days in the past.

Past work has shown that knowledge of the solar wind speed upstream of the Earth can be used to predict—in a linear or nonlinear filter sense—the subsequent fluxes of energetic electrons in the radiation belts (see Baker et al., 1990; Vassiliadis et al., 2002; Rigler et al., 2004). In Fig. 2 we illustrate the magnetosphere and the trapped radiation belts in the inner part of the system. As shown by the color-coded data plot of electron fluxes for various L-shells versus time (1999–2000), SAMPEX provides a broad, continuous measurement of the outer Van Allen belt electron

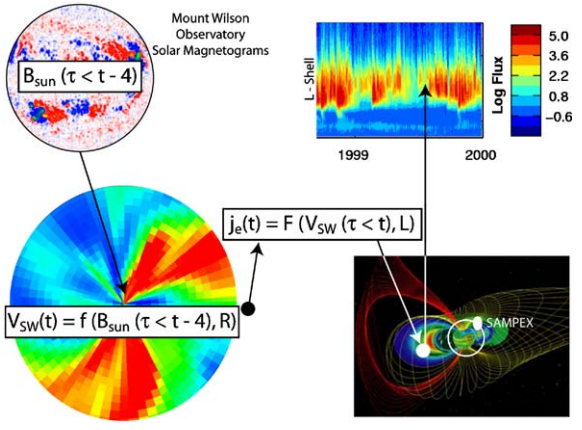

Fig. 2. Several of the key elements of the linked Sun-to-magnetosphere models and observations being developed for CISM including the solar magnetograms which provide the basis for $V_{SW}(t)$ estimates using the WSA model. The V_{SW} values are convolved with magnetospheric filters to predict L-dependent radiation belt electron fluxes as discussed in the text.

population (see, e.g., Baker, 1998; Li et al., 2003). Observations from SAMPEX, various operational geostationary orbit spacecraft, or other satellite data can be compared with the forecasted fluxes derived from a prediction filter that uses previous measurements or predictions of V_{SW} as suggested in Fig. 2:

$$J_e(t) = F(V_{SW}(\tau < t-4), L). \quad (2)$$

This equation states that the predicted daily-average flux of electrons, J_e, at a particular L-value in the magnetosphere at time, t, is determined through the filter operator, F, which utilizes the V_{SW} values derived from actual measurements or by using the WSA method.

In this work we use the 1995 WSA prediction of V_{SW}. That year was chosen because there were many high-speed streams, which are the solar wind structures that the WSA model best predicts. However, the interval was not ideal for the WSA model because there were approximately 10 days where solar observatory data were not available. Also, in 1995 the heliospheric current sheet was flat, which makes stream structures more difficult to predict (Arge and Odstrcil, 2004). Fig. 3a shows these data compared with daily-averaged L1 data. On the time scale in the figure it is clear that the overall structure is captured rather well. However, as shown in Fig. 3b, significant errors in the arrival time of the high-speed solar wind exist. Evaluation of the full year of data shows that the timing error is randomly distributed with a mean of zero and standard deviation of approximately 2 days.

3. Prediction models: 30–60 minute lead time

In this section, we develop linear filter models that predict log (J_e) based on V_{SW} at L1. In all cases the averaging time scale is one day. The linear filter method applied to J_e prediction using V_{SW} as an input was first considered by Baker et al. (1990). This inverse modeling method is based on the supposition that at least part of the dynamics of J_e is derivable from a linear ordinary differential equation (ODE) with V_{SW} as the driver. If this is the case, then the effective ODE can be derived from a historical data set of V_{SW} and J_e. This data-derived (or inverse) model contains information about the system dynamics, and it can be probed to determine physical properties of the system. One of these properties is the impulse response function (IRF). The IRF tells us how the system would respond if a unit impulse were given as the input (see Baker et al., 1990 and references therein).

As shown in Fig. 4(a), at $L = 6.6$, the derived model predicts that a 1-day pulse of V_{SW} would result in a sharp dropout of $j_e(\equiv \log J_e)$ and then a rise over 2 days and finally a decay over 4 days. The IRF for $1 \leqslant L \leqslant 10$ was computed by Vassiliadis et al. (2002) and is shown

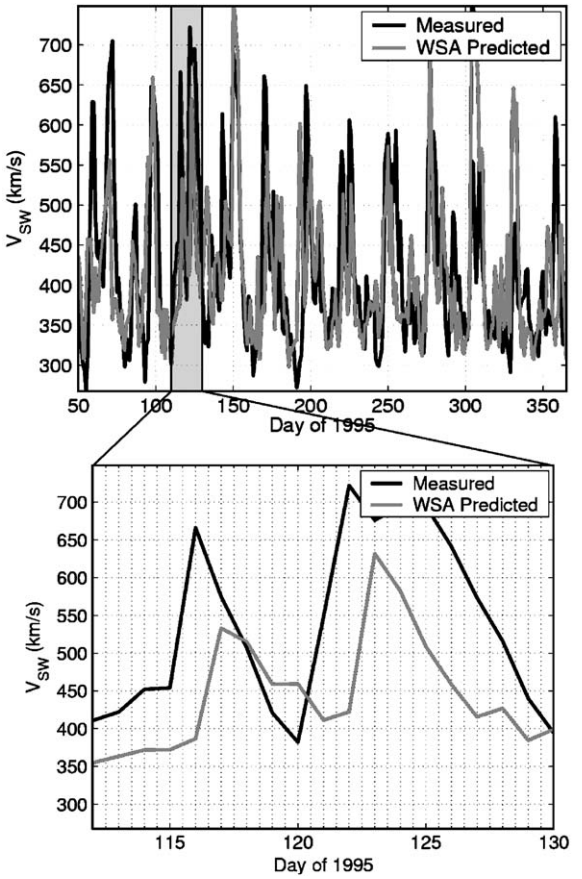

Fig. 3. (a) (top). Comparison of the WSA model prediction of V_{SW} at L1 (averaged to 1-day) with daily-averaged L1 measurements of V_{SW}. In 1995, the data-model correlation was 0.36 and the prediction efficiency was 0.13. (b) (bottom). Zoom-in of selected days in 1995. The WSA model clearly captures the large-scale trend, but errors in the arrival time are on the order of ±2 days.

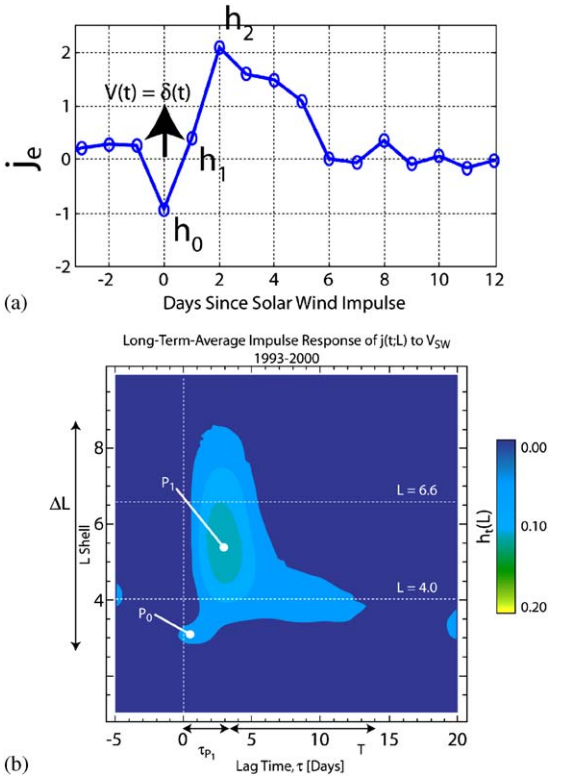

Fig. 4. (a) Impulse response function at $L = 6.6$; $h_0, h_1, \ldots$ are the coefficients of the impulse response function $j_e(t) = h_0 V(t-1) + h_1 V(t-2) + \cdots$. (b) Impulse response function (h_t) of $j_e(\equiv \log J_e)$ for $1 \leqslant L \leqslant 10$ (from Vassiliadis et al., 2002). P_0 and P_1 are the locations of local maxima in the impulse response function.

in Fig. 4b; the effective dynamical system, as represented by the IRF, has a strong dependence on L. This set of results, for all relevant L-shells, would allow one to forecast the electron flux throughout the entire radiation belt region by convolving the filter values with an input solar wind time series.

4. Prediction models: >1 day lead time

In this section we extend the methods described in the previous section so that the filters now predict j_e based on old measurements of V_{SW} at L1, V_{SW} predictions made by the WSA method, and old measurements of j_e. We seek to determine how effective each of these inputs is in predicting j_e.

The first experiment is shown schematically in Fig. 5(a). A linear filter model is computed for each of three separate inputs. The output of each filter is a prediction of j_e based only on preceding values of the superscripted quantity. A different filter is computed for lead times between 0 and 4 days. For the 0-day lead time, we determine the individual set of parameters, a, w, m that give the highest data-model correlation, with $T = 30$.

$$j_e^{L1}(t) = a_1 V^{L1}(t-1) + a_2 V^{L1}(t-2) + \cdots + a_T V^{L1}(t-T),$$

$$j_e^{WSA}(t) = w_1 V^{WSA}(t) + w_2 V^{WSA}(t-1) + \cdots + w_T V^{WSA}(t-T),$$

$$j_e^{MEAS}(t) = m_1 j_e(t-1) + m_2 j_e(t-2) + \cdots + m_T j_e(t-T). \quad (3)$$

The flux data set is from the SAMPEX Proton Electron Telescope from 1995–2001 (see Baker, 1998 and

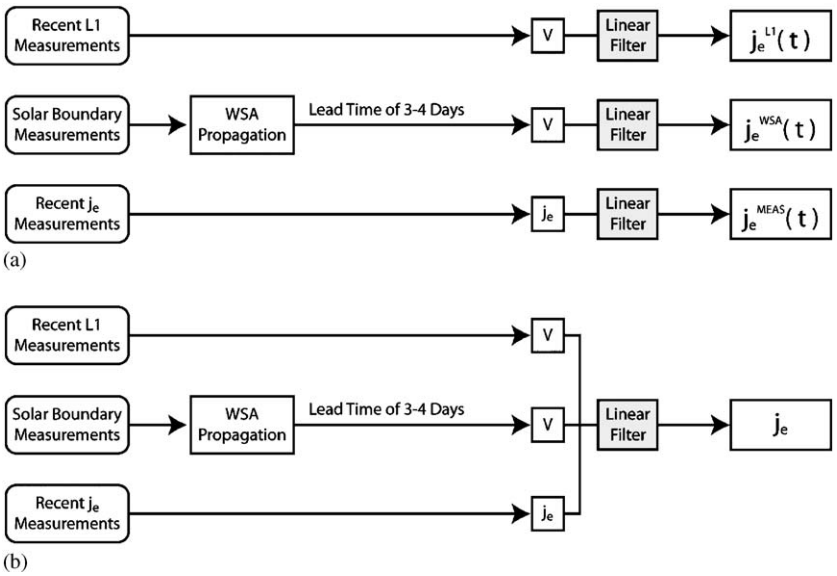

Fig. 5. (a) Each measurement (or prediction) is used to derive a linear filter that predicts j_e; (b) All measurements and predictions are used as inputs to a single linear filter that predicts j_e.

references therein). The daily-averaged solar wind velocity data are from the OMNI database of the National Space Science Data Center during the same time interval. The results of this are summarized in the middle three rows of Table 1.

The best 0-day lead time PE (defined as 1.0 minus the ratio of the mean square error of the prediction to the variance of j_e) is obtained from the filter that uses previous measurements of j_e (this is called an auto-regressive filter). Next, in importance, are previous measurements of V_{SW} made at L1. The WSA model always provides only 3–4 day lead times, so it has no entry in this or other short lead-time columns. The 1-day prediction efficiencies were determined by setting a_1 and m_1 in (Eq. (3)) to zero, and then re-computing the parameters $(a_2 \ldots a_t)$ and $(m_2 \ldots m_t)$ to maximize the data-model correlation. This procedure is repeated for the 2-, 3-, and 4-day columns. As the lead time increases, both methods exhibit poorer performance, with the j_e^{MEAS} PEs falling off much more quickly than the j_e^{L1} PEs. This residual prediction efficiency is due to the 2–3 day delay in the peak of the j_e response to V_{SW}; at the peak of j_e, what is most important is the amplitude of V_{SW} 2–3 days prior, as shown in the impulse response function of Fig. 4(a).

In the 4-day column we see that the j_e^{MEAS} and j_e^{L1} filters have a better prediction efficiency than the j_e^{WSA} filter. However, the difference is small, indicating that as the WSA PE of V_{SW} rises above its current value of 0.13 we are likely to see it provide predictions that are superior to what is possible using 3–4 day old measurements of j_e and V_{SW} at L1.

Table 1
Prediction efficiencies of the individual linear filter models (as in Fig. 6a) are shown along with the PE obtained from the combined method (Fig. 6b). The lead time of WSA is fixed at 3–4 days

Using alone	PEs at $L = 6.6$ (day)				
	0	1	2	3	4
WSA	—	—	—	0.05	0.05
L1	0.29	0.29	0.24	0.17	0.13
MEAS	0.53	0.22	0.12	0.09	0.07
Combined	0.58	0.36	0.27	0.20	0.17

In the final experiment, we take the V_{SW} prediction of the WSA model, old values of V_{SW}, and old values of J_e and combine them into a single filter that predicts $J_e(t)$. The results of this are shown in the last row of Table 1. For the 0-day column, the PE of the combined model is only slightly higher than that obtained from the J_e^{MEAS} model. This indicates that J_e^{MEAS} has the highest relative information content for specifying J_e at a 0-day lead time. In the last column, the PE from J_e^{L1} is only slightly less than that of the combined model, indicating that 4-day delayed measurements at L1 have the highest relative information content.

The analysis performed in this section is useful for obtaining an intuitive understanding of the relative importance of measured or predicted quantities that have either a causal connection or correlation with a quantity to be predicted. From this analysis it is clear

that old measurements of V_{SW} and j_e both have information useful in predicting j_e; this indicates that data assimilation methods may improve the predictability of j_e. The method outlined in Fig. 5(b) has similarities with data assimilation in that many measurement sources contribute to the final prediction and their influence is weighted. However, the term data assimilation is usually reserved for filters that have a specific mathematical form, such as the Kalman filter (Jazwinski, 1970).

5. Summary

We have shown that positive prediction efficiency can be obtained by driving a model of the daily-averaged $E>2$ MeV electron fluxes in the radiation belts with a prediction of the solar wind speed. This end-to-end coupling allows for 3–4 day lead time prediction. The relative importance of other measurements at 3–4 day lags was considered by developing filter models that used such measurements as inputs. It was found that 3–4 day old measurements of the solar wind velocity at L1 were able to provide prediction efficiencies in the prediction of MeV electron fluxes that were slightly higher than the PE provided using prediction of V_{SW} at the Earth. However, we foresee improvements in the WSA method that will probably substantially improve our 3–4 day forecasting ability.

Among the improvements foreseen would be changes in how individual data sets at the solar source surface are used. Currently, different solar magnetogram data sources are used individually; data from an individual solar observatory are used as boundary conditions to compute an equilibrium solution via the Wang–Sheeley method. A more complete analysis will involve tests to determine how predictions based on different data sources can be combined to yield improved predictions. A second possibility is to test interpolation schemes for their ability to give improved forecasts in between the forecast update times (approximately 8 hours, corresponding to the time between solar observation updates). A third possibility will be to use a data assimilation method to keep the WSA forecast "on track". A first approach of this sort will involve using L1 solar wind measurements to continually adjust and correct the solar wind forecasts via a feedback method.

We have only considered prediction of energetic electron fluxes in this paper. Statistically, j_e is driven primarily by the solar wind velocity (see Baker, 1998) in the sense that inverse models that use variables other than V_{SW} as an input to predict j_e are only slightly better than models that use only V_{SW} as an input. Many other parameters and indices are of interest for such long lead time. Currently the best-predicted Sun–Earth quantity is the solar wind velocity. For this reason, processes that have a high degree of predictability using only V_{SW} will be the best predicted in the near future by the method shown here.

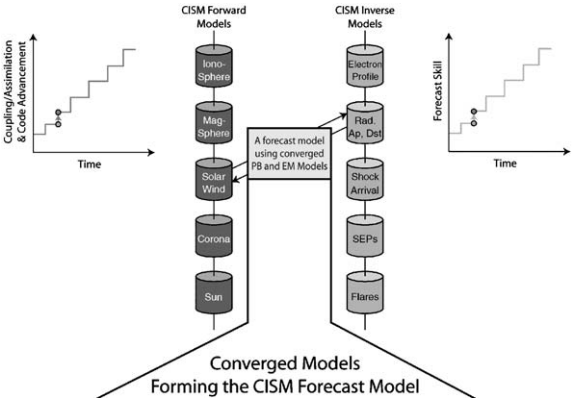

Fig. 6. The coupled forward models (left) and the coupled inverse models (right) being developed within CISM. These two approaches support and inform one another leading to continuous improvement. These models converge in order to form the CISM Forecast Model (FM) which builds upon elements of both the forward and inverse methods.

The analysis presented here forms some of the baseline testing of models that will be a part of the first-generation CISM forecast model. Fig. 6 demonstrates the relationship between the CISM forward models (e.g., MHD), the CISM inverse (e.g., filters or data-derived models, empirical, or semi-empirical models) and the CISM forecast model. The performance of the first-generation forecast model will be used as a benchmark. The CISM forward models that are able to predict a quantity of forecasting interest, or are able to exceed the performance of an existing model in the forecast chain, will be integrated into the forecast model. It is anticipated that the forward and inverse models will work in a competitive and complementary way in forming the forecast model. That is, in some cases a model that uses one of these two approaches will replace another. In other cases one of the approaches will fill in a gap where the other is deficient.

Acknowledgments

This material is based upon work supported in part by CISM, which is funded by the STC Program of the National Science Foundation under Agreement Number ATM-0120950.

References

Arge, C.N., Odstrcil, D., 2004. Stream structure and coronal sources of the solar wind during the May 12, 1997 CME.

Journal of Atmospheric and Solar Terrestrial Physics, this issue.

Arge, C.N., Pizzo, V.J., 2000. Improvements in the prediction of solar wind in the prediction of solar wind conditions using near-real time solar magnetic field updates. Journal of Geophysical Research 105, 10465–10479.

Baker, D.N., 1998. What is space weather? Advances in Space Research 23, 1–7.

Baker, D.N., McPherron, R.L., Cayton, T.E., Kebesadel, R.W., 1990. Linear prediction filter analysis of relativistic electron properties at 6.6 R_E. Journal of Geophysical Research 95, 15133–15140.

Jazwinski, A.H., 1970. Stochastic Processes and Filtering Theory. Academic Press, New York.

Li, X., Temerin, M., Baker, D.N., Reeves, G.D., Larson, D., Kanekal, S.G., 2003. The predictability of the magnetosphere and space weather. Eos Transactions of American Geophysical Union 84 (37), 369–370.

Luhmann, J.G., Solomon, S., 2004. Coupled model simulation of a Sun-to-earth space weather event. Journal of the Atmospheric and Solar Terrestrial Physics, this issue.

National Space Weather Strategic Plan, 1995. Off. Fed. Coord. for Met Services, NOAA, Silver Spring, MD.

Rigler, E.J., Baker, D.N., Weigel, R.S., Vassiliadis, D., Klimas, A.J., 2004. Adaptive linear prediction of radiation belt electrons using the Kalman filter. Space Weather 2, S03003 (doi:10.1029/2003SW000036).

Spence, H.E., Baker, D.N., Burns, A., Guild, T., Huang, C.-L., Siscoe, G., Weigel, R.S., 2004. Center for Integrated Space Weather Modeling metrics plan and initial validation results. Journal of the Atmospheric and Solar Terrestrial Physics, this issue.

Tsurutani, B.T., Baker, D.N., 1979. Substorm warnings: an ISEE-3 real time data system. Eos, Transactions of American Geophysical Union 60 (41), 702–703.

Vassiliadis, D., Klimas, A.J., Kanekal, S.G., Baker, D.N., Weigel, R.S., 2002. Long-term average, solar-cycle, and seasonal response of magnetospheric energetic electrons to the solar wind speed. Journal of Geophysical Research 107 (A11) doi:10.1029/2001JA000506.

Wang, Y.-M., Sheeley, N.R., Andrews, M.D., 2002. Polarity reversal of the solar magnetic field during cycle 23. Journal of Geophysical Research 107 (A12) doi:10.1029/2002JA009463.

Weigel, R.S., Klimas, A.J., Vassiliadis, D., 2003. Solar wind coupling to and predictability of ground magnetic fields and their time derivatives. Journal of Geophysical Research 108 (A7) doi:10.1029JA009627.

Wiltberger, M.J., Wang, W., Burns, A., Lyon, J.G., Solomon, S., 2004. Initial results from the coupled magnetosphere–ionosphere–thermosphere model: magnetospheric and ionospheric responses. Journal of the Atmospheric and Solar Terrestrial Physics, this issue.